AIAA JOURNAL
Vol. 33, No. 5, May 1995

Adaptive Grid Scheme for Vortex-Induced Boundary Layers

E. C. Adams* and A. T. Conlisk†
Ohio State University, Columbus, Ohio 43210
and
F. T. Smith‡
University College, London WC1E 6BT, England, United Kingdom

An adaptive-grid scheme is developed to resolve extremely large gradients associated with an unsteady vortex-induced boundary-layer flow. Previous investigations based on Eulerian descriptions have failed to resolve the terminal structure of the flowfield due to the emergence of a singularity at a finite time. The present approach is based on a moving-grid method applied to the streamwise direction of the boundary layer. Grid movement is coupled to the flowfield in an autonomous manner by an analytical weight function designed to improve the numerical stability and computational efficiency of the algorithm. The time and location of the singularity are successfully predicted in agreement with previous published Lagrangian calculations and asymptotic analysis.

Introduction

ACCURATE solutions of complex unsteady viscous flow problems of practical engineering interest often are impractical or even impossible using conventional Eulerian grid and solution techniques. The use of adaptive-grid methods is one way of improving the numerical accuracy and computational efficiency in these situations. Adaptive-grid methods are characterized by the careful organization of grid points into regions of the flowfield that exhibit rapid variations in the spatial dimensions and/or time. To justify the cost of managing an adaptive-grid scheme, the methods are typically applied to physical problems that possess a wide range of length and/or time scales. Applications include shock impingements, traveling waves, and flame propagation. In the present work, an adaptive-grid scheme is developed for a vortex/solid boundary interaction problem, although the fundamental concepts apply to many other types of partial and ordinary differential equations.

The classical noninteracting unsteady boundary layer induced by a rectilinear vortex above a plane wall in an otherwise stagnant medium is considered, following the seminal formulation by Walker.[1] The problem is a model for the type of unsteady separation that occurs in a variety of practical applications including vortex interactions associated with rotorcraft, dynamic stall, and flows in turbomachinery. More recently, the eruptive nature of the flow has been suggested as a fundamental mechanism in the transition to turbulence.[2]

Significant numerical difficulties associated with this problem arise due to the sudden development of extremely small length and time scales. As the vortex interacts with the wall, a region of recirculating flow emerges close to the wall in the form of a secondary vortex, and subsequently a thin shear region develops perpendicular to the wall. Numerical issues are further complicated by the emergence of a singularity in the boundary-layer equations at a finite time due to an adverse pressure gradient imposed on the boundary layer by the vortex. The singularity is accompanied by a rapid increase in the thickness of the boundary layer, and consequently severe gradients emerge that are not detected by previously employed Eulerian methods.[1,3]

It is generally accepted that the Moore–Rott–Sears (MRS) model for unsteady separation gives the required conditions for a singularity to occur.[4] This model has been validated numerically by Van Dommelen and Shen,[5] who performed a calculation of the impulsively started cylinder in a Lagrangian coordinate system. In contrast to the standard Eulerian approach, the velocity and position of fluid particles are computed as a function of an initial distribution of particles. In the Lagrangian formulation, the singular variables, normal velocity v and coordinate y, are not included in the momentum equation, and so the calculation proceeds in terms of the nonsingular streamwise velocity u, thereby making the scheme more robust. For the vortex-induced boundary-layer problem considered here, the time and location of the singularity is uniquely determined, albeit with some difficulty, by the Lagrangian approach of Peridier et al.[6] The structure of the singularity is in fact generic for most types of two-dimensional unsteady eruptive boundary layers.[7]

Previous attempts to employ an adaptive-grid scheme for the eruptive type of flowfields considered here are few (see Vickers and Smith[8]). For the type of vortex-induced boundary-layer problems considered here, it is recently concluded by Doligalski et al.[2] that it is "essentially impossible to accurately resolve the phenomena involved using conventional methods based on the Eulerian description of the fluid motion," and when considering an adaptive grid, "the construction of an appropriate Eulerian algorithm is very challenging." The terminal structure of the present problem has not been resolved in previous investigations using an Eulerian scheme.

The present adaptive-grid scheme is based on a moving-grid approach in which the total number of grid points is conserved. The governing equations are solved directly in the physical plane, as opposed to the more conventional approach in which the governing equations are transformed to a uniformly spaced fixed grid.[8,9] The movement of grid points is coupled to the physical solution by a weight function.[10] The conventional approach for obtaining the weight function with numerical techniques is found to be ineffective once the spikelike behavior is initiated. Consequently, an "analytical weight function" is formulated,[11] leading to a robust and successful calculation.

Problem Statement

The adaptive-grid method considered here is applied to the vortex-induced boundary-layer problem as formulated by Walker.[1] Two rectilinear point vortices are situated in an otherwise stagnant medium and separated by a distance $2a$ with equal strengths κ and opposite rotations as shown in Fig. 1; the vortices induce a velocity $V = \kappa/2a$ on each other in the positive x direction. At $t = 0$, the plane of symmetry is impulsively replaced by a solid boundary, and consequently an unsteady boundary layer is formed to satisfy the no-slip condition at the wall. The computational domain is defined by a coordinate system moving with the vortex in the upper-half plane.

The inner viscous flow is governed by the unsteady boundary-layer equations, which here are made nondimensional using the

Received May 9, 1994; revision received Oct. 7, 1994; accepted for publication Oct. 10, 1994.

*Graduate Research Assistant, Department of Mechanical Engineering. Student Member AIAA.

†Associate Professor, Department of Mechanical Engineering. Senior Member AIAA.

‡Professor, Department of Applied Mathematics.

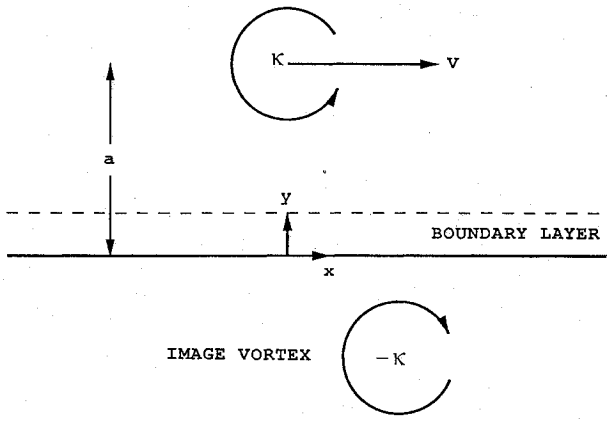

Fig. 1 Boundary layer induced by a rectilinear vortex.

characteristic length a and velocity V. The Reynolds number is $Re = Va/\nu$, where ν is the kinematic viscosity coefficient. Following Walker,[1] the infinite streamwise domain $x \in (-\infty, \infty)$ is compressed into a finite computational domain $\xi \in [2, 0]$ using a Gortler-type transformation. Rayleigh similarity variables $\eta = y/2\sqrt{t}$ and $\psi = 2\sqrt{t}\Psi$ are introduced, the edge velocity is defined by $U_e(\xi) = 2(1 - \cos\pi\xi)$, and the streamwise velocity component is expressed as the perturbation, $u = U_e(\xi)U - 1$. The governing equations expressed in the computational domain are the continuity equation

$$U = \frac{\partial \Psi}{\partial \eta} \tag{1}$$

and boundary-layer equation

$$4t\frac{\partial U}{\partial t} = \frac{\partial^2 U}{\partial \eta^2} + P\frac{\partial U}{\partial \eta} + Q\frac{\partial U}{\partial \xi} + RU + S \tag{2}$$

where

$$P = 2\eta + \frac{2t}{\pi}\left(U_\epsilon^2\frac{\partial \Psi}{\partial \xi} + U_e U_e'\Psi\right), \qquad Q = \frac{2t}{\pi}U_e(U_eU - 1)$$

$$R = \frac{2t}{\pi}U_e'(U_eU - 1), \qquad S = \frac{2t}{\pi}U_e'(1 - U_e)$$

subject to the boundary conditions,

$$U(\xi, 0, t) = \Psi(\xi, 0, t) = 0, \qquad U(\xi, \infty, t) = 1$$
$$U(0, \eta, t) = U(2, \eta, t) =, U(\xi, \eta, 0) = \text{erf}\eta \tag{3}$$

$$\Psi(0, \eta, t) = \Psi(2, \eta, t) = \Psi(\xi, \eta, 0) = \eta\text{erf}\eta + \frac{e^{-\eta^2} - 1}{\sqrt{\pi}} \tag{4}$$

Results of a conventional fixed-grid approach are summarized to demonstrate the numerical difficulties associated with the present problem. Using one processor of a Cray Y-MP8/864, a well vectorized calculation (200/250 Mflops) is performed using 721×241 grid points. The calculation terminates at $t = 0.848$ when the iteration scheme diverges; however, spurious solutions in the form of oscillations are evident as early as $t = 0.8$ on the downstream side of the secondary vortex, and oscillations are severe at $t = 0.84$ as shown in Fig. 2. (Fixed-grid results of Walker[1] using 181×121 grid points are considered inaccurate as early as $t = 0.7$.) The time $t = 0.8$ corresponds to the emergence of what is defined here as a perpendicular shear region within the boundary layer. It is concluded that accurate predictions of the flowfield for $t > 0.8$ are not possible using conventional fixed-grid methods. Clearly, many more grid points (and shorter time steps) are needed in the shear region to reach the singular time of $t_s = 0.989$ estimated by Lagrangian methods.[6]

Adaptive-Grid Method

The adaptive-grid method developed here is applied to the streamwise direction of the two-dimensional boundary-layer problem. Adapting in only the ξ direction is sufficient to resolve the entire

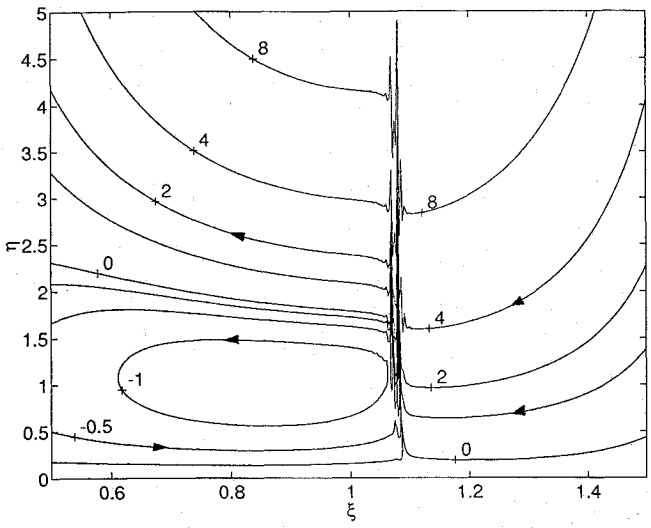

Fig. 2 Instantaneous streamlines at $t = 0.84$ using 721×241 fixed grid points.

flowfield accurately because gradients in the ξ direction are at least an order of magnitude larger than gradients in the η direction as the singular time is approached.

Moving-grid methods are designed to temper large gradients in the flowfield by clustering grid points into regions where they occur. By discretizing the governing equations directly in the physical plane, changes with respect to ξ are automatically accounted for by the approximations of the spatial derivatives, and it is only necessary to account for the movement of grid points. Expanding the velocity in the form of a Taylor series with respect to ξ and t, and neglecting terms of second order and higher, one can express the time derivative of the velocity at a moving grid point (denoted by i) as

$$\left(\frac{\partial U}{\partial t}\right)_i = \lim_{\Delta t \to 0}\frac{U_i^{n+1} - U_i^n}{\Delta t} = \left(\frac{\partial U}{\partial t}\right)_\xi + \left(\frac{\partial U}{\partial \xi}\right)_t\frac{\Delta \xi}{\Delta t} \tag{5}$$

In the limit $\Delta t \to 0$, the original form of the time derivative term is expressed as

$$\left(\frac{\partial U}{\partial t}\right)_\xi = \left(\frac{\partial U}{\partial t}\right)_i - \left(\frac{\partial U}{\partial \xi}\right)_t\frac{d\xi_i}{dt} \tag{6}$$

By substituting Eq. (6) into Eq. (2), one can express the governing boundary-layer Eq. (2) by

$$4t\frac{\partial U}{\partial t} = \frac{\partial^2 U}{\partial \eta^2} + P\frac{\partial U}{\partial \eta} + \left(Q + 4t\frac{d\xi_i}{dt}\right)\frac{\partial U}{\partial \xi} + RU + S \tag{7}$$

and it is emphasized that only one additional term is introduced by the transformation.

Numerical Methods

The differential Eq. (7) is discretized according to a conventional Crank–Nicolson method using standard second-order central differencing for the η direction and second-order central differencing for arbitrary grid spacing in the ξ direction,

$$4t\left(\frac{U_i^{n+1} - U_i^n}{\Delta t}\right)\frac{U_{i,j+1}^{n+\frac{1}{2}} - 2U_{i,j}^{n+\frac{1}{2}} + U_{i,j-1}^{n+\frac{1}{2}}}{(\Delta\eta)^2}$$
$$+ P\left(\frac{U_{i,j+1}^{n+\frac{1}{2}} - U_{i,j-1}^{n+\frac{1}{2}}}{2\Delta\eta}\right) + \left[Q + 4t\left(\frac{\xi_i^{n+1} - \xi_i^n}{\Delta t}\right)\right]$$
$$\times\left[\frac{\xi_b^2 U_{i+1}^{n+\frac{1}{2}} + (\xi_f^2 - \xi_b^2)U_i^{n+\frac{1}{2}} - \xi_f^2 U_{i-1}^{n+\frac{1}{2}}}{\xi_f\xi_b\xi_c}\right] + RU_{i,j}^{n+\frac{1}{2}} + S \tag{8}$$

Table 1 Time steps, relaxation factors for the flow (λ_U) and grid (λ_ξ), and approximate number of iterations per time step for the flow (I_U) and grid (I_ξ) for an adaptive-grid solution using 721 × 241 grid points

t	Δt	λ_U	λ_ξ	I_U	I_ξ
0.00	0.0010	1.0	1.0	2	2
0.01	0.0020	1.0	1.0	3	4
0.40	0.0010	0.8	1.0	12	8
0.70	0.0010	0.6	0.5	18	18
0.85	0.0005	0.4	0.5	24	40
0.90	0.0002	0.3	0.5	36	90
0.95	0.0001	0.2	0.5	90	200
0.96	0.0001	0.1	0.25	250	230

where

$$\xi_f = \xi_{i+1}^{n+\frac{1}{2}} - \xi_i^{n+\frac{1}{2}}, \qquad \xi_b = \xi_i^{n+\frac{1}{2}} - \xi_{i-1}^{n+\frac{1}{2}}$$

$$\xi_c = \xi_{i+1}^{n+\frac{1}{2}} - \xi_{i-1}^{n+\frac{1}{2}}$$

and all of the coefficients are approximated at the $n + \frac{1}{2}$ time step by simple average. The spatial indices i and j vary from 0 to M and 0 to N corresponding to the streamwise and normal directions, respectively. The grid spacing $\Delta\eta = \eta_\infty/N$ is uniform, where η_∞ is set to a finite value large enough (here $\eta_\infty = 9$) such that variations in the solution are no longer significant. Initially, spacing in the ξ direction also is uniform, $\Delta\xi = 2/M$. The time steps Δt are varied throughout the integration (see Table 1). The boundary conditions, Eqs. (3) and (4), and the continuity Eq. (1) are unaffected by the adaptive-grid formulation.

The difference Eq. (8) is linearized by updating the coefficients of the nonlinear terms using a block-iterative scheme. An efficient scheme is employed in which the Thomas algorithm is used to solve U directly along lines of constant ξ. To vectorize the data-dependent algorithm, the operations of the Thomas algorithm are performed on vectors of grid points along lines of constant η. The result is a Jacobi-type iterative scheme with under-relaxation applied at later times. The Ψ array is updated by integration of U according to Simpson's rule.

Grid Equation

The nonuniform distribution of grid points in the physical plane is defined by the equidistribution statement

$$c\,\mathrm{d}\zeta = W(\xi, t)\,\mathrm{d}\xi \tag{9}$$

where $W(\xi, t)$ is a weight function, c is an undetermined constant, and ζ represents a uniform distribution of grid points corresponding to grid points in the physical plane.[10] The left-hand side of Eq. (9) is constant, and therefore large values of the weight function correspond to small grid spacing in the physical plane and vice versa.

There are several ways to extract numerical values for the location of grid points from the grid equation (9). In the present work, a numerical integration of Eq. (9) is used to determine the location of the grid points in the physical plane at each time step. The local integration of Eq. (9) across a pair of neighboring grid points in the ξ coordinate is expressed as

$$c\int_{\xi_{i-1}}^{\xi_i} \mathrm{d}\zeta = \int_{\xi_{i-1}}^{\xi_i} W(\xi)\,\mathrm{d}\xi \tag{10}$$

$$c\int_{\xi_i}^{\xi_{i+1}} \mathrm{d}\zeta = \int_{\xi_i}^{\xi_{i+1}} W(\xi)\,\mathrm{d}\xi \tag{11}$$

The trapezoidal rule is used to approximate the integrals on the right-hand sides of Eqs. (10) and (11),

$$c\Delta\zeta = \tfrac{1}{2}[W(\xi_i) + W(\xi_{i-1})](\xi_i - \xi_{i-1}) + \mathcal{O}(\Delta\xi)^3 \tag{12}$$

$$c\Delta\zeta = \tfrac{1}{2}[W(\xi_{i+1}) + W(\xi_i)](\xi_{i+1} - \xi_i) + \mathcal{O}(\Delta\xi)^3 \tag{13}$$

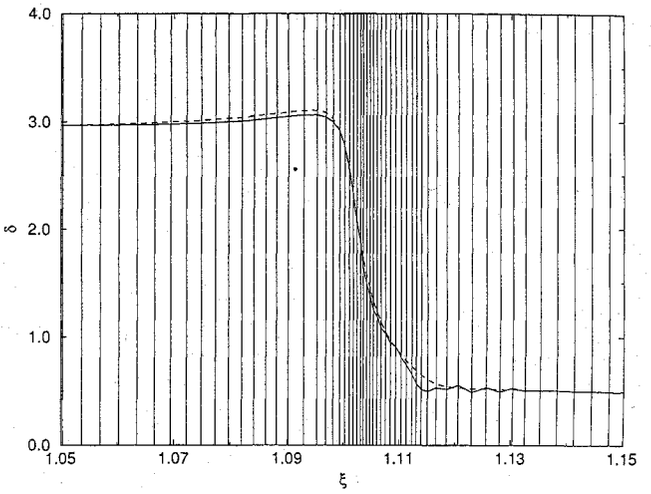

Fig. 3 Adaptive-grid solution using a numerical weight function (solid) with baseline solution (dashed) for the displacement thickness at t = 0.8985 with 721 × 241 grid points, denoted by vertical lines.

Setting both expressions equal to the same constant $2c\Delta\zeta$ and therefore equal to each other, a single tridiagonal system of equations is derived,

$$[W(\xi_i) + W(\xi_{i-1})]\xi_{i-1} - [W(\xi_{i-1}) + 2W(\xi_i) + W(\xi_{i+1})]\xi_i + [W(\xi_i) + W(\xi_{i+1})]\xi_{i+1} = 0 \tag{14}$$

subject to the boundary conditions ξ_0 and $\xi_N = 2$.

The nonlinear system of equation (14) is linearized by updating the coefficients in an iterative manner and solved using the Thomas algorithm. A relative convergence test is defined by

$$\max\left(\left|1 - \frac{\xi_i - \tilde{\xi}_{i-1}}{\tilde{\xi}_i - \xi_{i-1}}\right|\right) < \epsilon \tag{15}$$

where $\epsilon = 10^{-4}$ and the tildes denote values from the previous iteration. A relative convergence test is especially important for adaptive-grid schemes for which the grid spacings across the spatial domain can vary by several orders of magnitude (see Fig. 3).

Numerical Weight Functions

The most challenging aspect of the present problem is the development of an effective weight function for coupling the movement of grid points to variations in the flowfield, especially as the singular time is approached. The conventional approach is to couple the movement of grid points directly to one or more components of the numerical solution. Many different type of numerical weight functions were considered in the present study[11]; a representative form is

$$W(\xi, t) = [F^2(\xi, t) + 1]^\alpha \tag{16}$$

where α is a free parameter and $F(\xi, t)$ is the component of the flow solution that is used as the metric for the adaptive-grid scheme. Several choices for $F(\xi, t)$ were considered: U_ξ, the instantaneous gradient of the perturbed external velocity; v_e, the "blowing" velocity at the edge of the boundary layer; and δ_ξ^*, the slope of the displacement thickness.

Using 361 × 181 grid points, all of the numerical weight functions provide accurate results for later times than the 721 × 241 fixed-grid solution, which is inaccurate for $t > 0.8$; however, all of the numerical weight functions fail before $t = 0.91$, once the spikelike behavior in the shear region is initiated. The problem is illustrated in Fig. 3, which shows results typical of adaptive-grid solutions based on numerical weight functions. The solid line in Fig. 3 shows the displacement thickness in the shear region for a calculation obtained using $F = \delta_\xi^*$ and $\alpha = 0.15$ in Eq. (16). Note the presence of oscillations in displacement thickness on either side of the shear region.

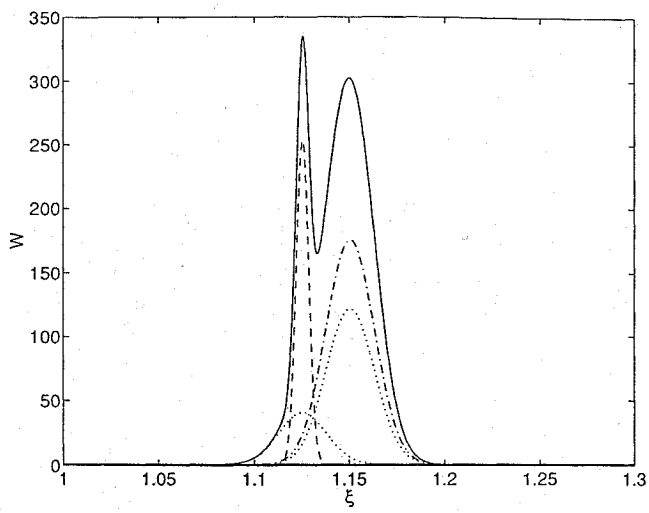

Fig. 4 Analytical weight function (solid) at $t = 0.97$ with individual Gaussian functions G_1 (dashed), G_2 (dash-dotted), and G_3 and G_4 (dotted).

It is suggested that numerical weight functions fail to provide accurate solutions for times $t > 0.9$ because weight functions based on Eq. (16) are incapable of accounting for more than one type of rapid variation in the flow solution. For example, the slope of the displacement thickness is not large at $\xi = 1.12$ as shown in Fig. 4, and therefore the numerical weight function based on $F = \delta_\xi^*$ does not direct enough grid points into that region. Consequently, the oscillations are allowed to grow rapidly on the downstream side of the shear region at $t = 0.8985$, and suddenly at $t = 0.9$ the numerical scheme fails to converge. In theory, it may be possible to construct a more sophisticated numerical weight function based on a combination of many different gradients in the flowfield, but in practice it is expected that a function that permits stable calculations might not be computationally efficient due to the algorithmic complexity that would be required.

Analytical Weight Function

The deficiencies of a numerical weight function are overcome by using an analytical weight function. The term "analytical weight function" is used to refer to a weight function for which part or all of the behavior of the numerical solution is represented by analytical functions.[11] The functions used to construct an analytical weight function may be derived directly from the numerical solution, either implicitly or explicitly, or from entirely independent analysis of the governing flow equations. Regardless of how it is constructed, one of the useful properties of an analytical weight function is that it is a continuous function (as opposed to the evaluation of a numerical weight function at a finite number of points), even though it is usually necessary to discretize the analytical weight function to solve the grid equation (in some cases it may be preferable to solve Eq. (9) analytically). In addition, the analytical weight function generally allows for a more autonomous coupling between the movement of grid points and the physical solution, which improves the numerical stability and computational efficiency of the gridding algorithm.

The analytical weight function used here is constructed from the superposition of four analytical functions and an arbitrary positive constant,

$$W(\xi, t) = G_K + 1 \tag{17}$$

where $G_k (k = 1, 2, 3, 4)$ are Gaussian functions of the form,

$$G_k = (t_s^* - t)^{-\alpha_k} \exp\left\{ - \frac{\beta_k[\xi_c(t) + \gamma_k - \xi]^2}{(t_s^* - t)^3} \right\}$$

and α_k, β_k, γ_k, and t_s^* are all nonnegative free parameters. In the present calculations, $\beta_4 = \beta_3$, $\gamma_3 = \gamma_1 = 0$, and $\gamma_4 = \gamma_2$, and so there are a total of nine free parameters in the four functions G_k. The term $\xi_c(t)$ is a translation function associated with the location of intense variations in the solutions and is determined dynamically

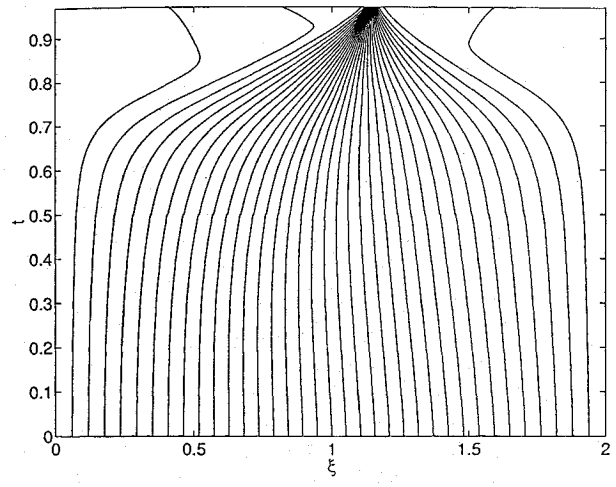

Fig. 5 Trajectories of grid points; every 20th grid point of 721 is plotted.

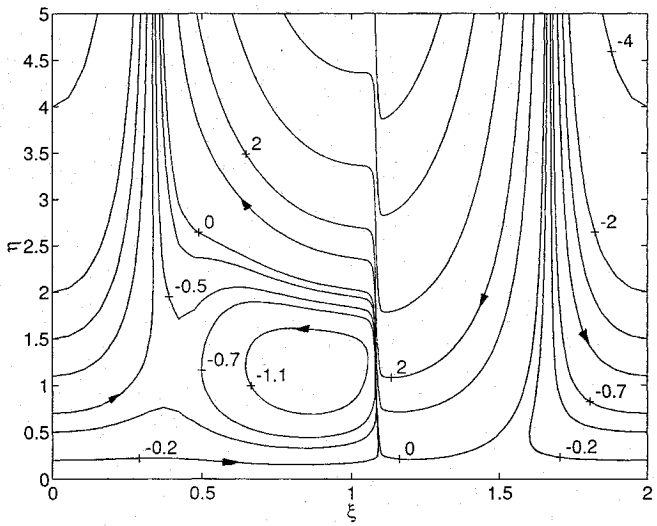

Fig. 6 Instantaneous streamlines at $t = 0.97$.

as described later. The magnitude of a Gaussian function increases as α_k increases, and the shape of the function sharpens as β_k increases. A construction of the weight function is illustrated in Fig. 5 at $t = 0.97$, for example, from which it may be concluded that $\alpha_1 > \alpha_2$ and $\beta_1 > \beta_2$.

The free parameter t_s^* is an estimated singular time ($t_s^* > t_s$) that determines the upper limit on the time domain of the integration. The grid is the most sensitive to t_s^*; the grid is compressed more tightly into the shear region as t_s^* is chosen closer to t_s. The value t_s^* should be established first and is determined iteratively for problems in which t_s is not known from other results. Indeed, we are now producing solutions for the interacting boundary-layer problem for the impulsively started cylinder for which t_s is unknown, and the results will be reported in a future paper.

Components G_1 and G_2 are designed to account for two separate types of severe gradients that occur within the shear region, whereas components G_3 and G_4 are added strictly to improve the numerical stability of the grid equation (14). Component G_1 is designed to account for gradients associated with spikelike singular behavior in the flowfield (see Fig. 6). The center (maximum value) of G_1 is at $\xi = \xi_c(t)$; for this reason $\gamma_1 = 0$. Component G_2 is designed to account for rapid variations in the flowfield that are due to an unknown combination of gradients in the flowfield (oscillations due to these gradients are observed near $\xi = 1.12$ in Fig. 4, for example). The location of G_2 is offset from G_1 by the free parameter γ_2. The origin of the gradients is attributed to the nonlinearity of the boundary-layer equations as well as two-dimensional effects of the spatial domain. Numerical weight functions are inherently too restrictive to account

for such complex and unclearly defined gradients in the numerical solution.

Components G_3 and G_4 improve the stability of the grid equation by keeping the grid spacing ratio, defined by the discrete function $\chi_i = (\xi_{i+1} - \xi_i)/(\xi_i - \xi_{i-1})$, close to unity. An abrupt rise in the weight function can cause the grid equation to diverge (typically for $\chi_i < \frac{1}{3}$ or $\chi_i > 3$). The components G_3 and G_4 complement G_1 and G_2 for this reason, $\gamma_3 = \gamma_1$ and $\gamma_4 = \gamma_2$, respectively in Eq. (17).

The location of G_1, defined by $\xi_c(t)$, is determined in an iterative manner from the numerical solution and does not require a priori knowledge. At each time step, the streamwise location of the shear region (denoted by a spike in the displacement thickness δ^*) is recorded from the numerical solution; the maximum value of δ^*_ξ is used for times before the emergence of spikelike behavior. Smooth grid point trajectories are essential to prevent grid oscillations from interfering with inherently sensitive spikelike behavior in the flowfield; therefore the numerical data are fit to a third-order polynomial for $\xi_c(t)$. The coefficients of the polynomial are updated at each iterative integration of the flowfield based on previous numerical results.

The free parameters of the analytical weight function are adjusted in an iterative manner based on numerical results of previous calculations (it is conceivable that the free parameters could be adjusted automatically, incorporating various degrees of sophistication). Several different sets of free parameters define grids that provide accurate flow solutions, and so it is not difficult to converge on a set of suitable values. The free parameters are independent of the grid size so that most of the iterations of free parameters may be performed on a coarse grid. As expected, the flow solution becomes increasingly more sensitive to the free parameters as the singular time is approached.

Results

All numerical results presented here are generated from an adaptive-grid solution using the analytical weight function, Eq. (17), with 721 × 361 grid points. The calculation fails at $t = 0.98$ due to a lack of grid points in the streamwise direction, but the solution is considered inaccurate for $t > 0.97$ when differences in comparison with coarse grids begin to diverge substantially. Richardson's extrapolated solutions using half the number of grid points in either the streamwise or normal directions are in agreement to at least two significant digits in the shear region and at least three digit elsewhere in the flowfield. Prediction of the singular time using the coarse grid differs by less than 1% compared with the 721 × 361 grid. The time steps, relaxation factors, and number of iterations per time step are listed in Table 2. Time steps were shortened as the number of iterations per time step increased but were not allowed to go below 10^{-4}. The results are in agreement with previously published Lagrangian results and asymptotic analysis as is discussed later.

Using first a 361 × 181 grid, and then the 721 × 361 grid, 10 iterative integrations of the flowfield were performed to obtain the free parameter values for the analytical weight function listed in Table 2. It was not necessary to adjust the free parameters to within more than two significant digits (excluding t_s^*). Perturbing the values listed in Table 2 by 1%, for example (including t_s^*), only changes the predicted singular time by 0.1%.

The trajectories of the grid points are plotted in Fig. 5, and it is emphasized that the trajectories are smooth and do not cross despite the fact that more than 85% of the original number of grid points are clustered into less than 5% of the streamwise domain at $t = 0.97$. At $t = 0.97$, the ratio of the largest grid spacing to the smallest grid spacing ($\Delta\xi_{\min} = 5.8 \times 10^{-5}$) is 345. The equivalent number of fixed-grid points based on the smallest grid spacing is 34,100, which suggests that more than 8 million grid points would be required to resolve the flowfield using a standard fixed-grid method with uniform grid spacing. Without estimating how much the time steps would have to be reduced to prevent the iterations from diverging, it is clear that an equivalent conventional fixed-grid scheme is impractical.

Computational Efficiency

One calculation of an adaptive-grid solution using 721 × 361 grid points requires a total of 1654 time steps and 7200 s of CPU time using one processor of a Cray Y-MP8/864 vectorized to execute at 200 Mflops. The computational burden required to manage the adaptive-gridding algorithm is estimated to be 23%, determined by comparing the CPU time required to perform adaptive-grid and fixed-grid calculations for the same grid size. In Table 3, the minimum number of adaptive-grid points are employed to achieve the same accuracy as a 721 × 241 fixed-grid solution for $0 \le t \le 0.8$. It is concluded that the adaptive-grid scheme requires less than one-tenth the amount of CPU time and one-eighth the number of grid points to obtain results comparable to a fixed-grid calculation and that the fixed-grid solution is inaccurate for $t > 0.8$.

Table 2 Free parameters of the analytical weight function

α_1	α_2	α_3	α_4	β_1	β_2	β_3	γ_2	t_s^*
1.5	1.4	1.0	1.3	0.7	0.05	0.05	0.025	0.995

Table 3 Computational efficiency of adaptive-grid vs fixed-grid calculation

Code	Grid size	CPU time, s
Fixed grid	721 × 181	245
Adaptive grid	91 × 181	20.0
Ratio	0.13	0.082

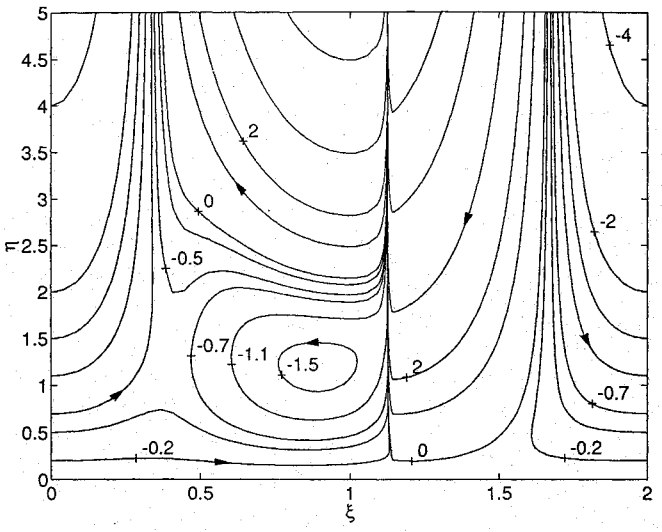

Fig. 7 Instantaneous streamlines at $t = 0.85$.

Physical Results

Oscillations in the fixed-grid solution at $t = 0.84$ in Fig. 2 are easily removed as shown in Figs. 6 and 7 and do not occur in the adaptive-grid solution until $t = 0.975$. The temporal development of the displacement thickness is plotted in Fig. 8, and the best results for alternative methods are noted. The distribution of vorticity in the boundary layer is represented by lines of constant vorticity ($\omega = -\partial u/\partial y$) plotted in Fig. 9. The Lagrangian results[6] as well as the adaptive-grid results here indicate that the secondary vortex is being drawn away from the wall and into an inviscid eruptive spike (an inviscid region of fluid within the shear region is indicated by a pinching of the zero-vorticity line). It is suggested by Peridier et al.[6] that the vortex may ultimately be ejected from the boundary layer as has been observed experimentally (see Doligalski et al.[2] and Harvey and Perry[12]).

Finite Time Singularity

It is well known that the solution of the present problem terminates with the emergence of the so-called separation singularity at a finite time. The adaptive-grid results may be used to confirm the structure of the singularity as predicted by previously published asymptotic analysis as well as the time and location of its occurrence.

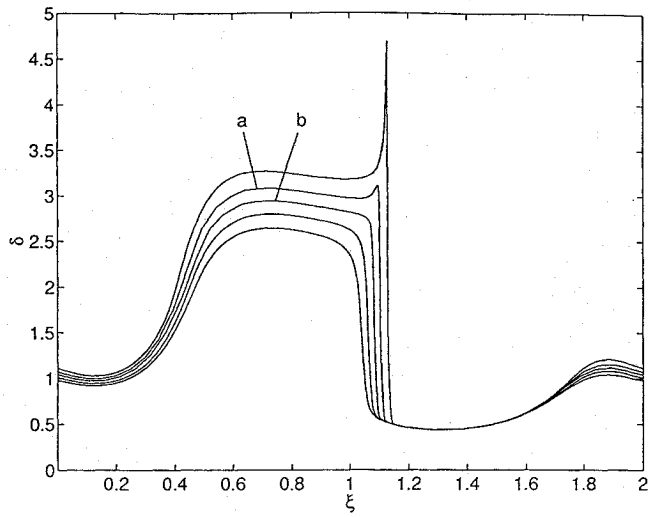

Fig. 8 Temporal development of displacement thickness δ^* at times $t = 0.75(0.05), 0.90$, and 0.97. Adaptive-grid results using a numerical weight function fail beyond a and fixed-grid results fail beyond b.

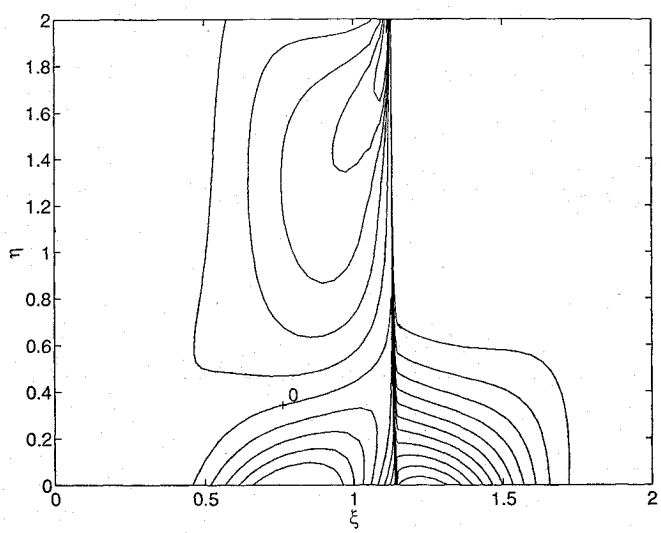

Fig. 9 Lines of constant vorticity at $t = 0.97$.

According to Van Dommelen and Shen[5] and Elliott et al.,[7] the maximum displacement thickness near the singular time is predicted to leading order by

$$\delta^*_{\max} \sim C(t_s - t)^{-\frac{1}{4}} \text{ as } t \to t_s \tag{18}$$

where C is a constant of $\mathcal{O}(1)$. To compare adaptive-grid results with the asymptotic model, Eq. (18) is written as

$$(\delta^*_{\max})^{-4} = at + b \tag{19}$$

where the shop is $a = -1/C^4$ and the intercept is $b = t_s/C^4$. The singular time and constant are estimated from a least-squares curvefit of numerical data to be $t_s = 0.991 \pm 0.008$ and $C = 1.81 \pm 0.004$, which compare well with Lagrangian results[6] of $t_s = 0.989$ and $C = 1.71 \pm 0.02$.

An independent estimation of the time and location of the separation singularity may be performed using the MRS condition, which stipulates that the occurrence of a singularity coincides with the simultaneous vanishing of the streamwise velocity and shear in a frame of reference moving with the separation phenomenon. Contours of the zero-velocity and zero-vorticity lines may be plotted at various times near the singularity. Because of the large number of grid points clustered in the region, it is possible to obtain accurate measurements of the distance between the zero-velocity and zero-vorticity lines using graphical methods. From a linear curvefit of the data, the results are extrapolated to determine when the zero-velocity and zero-vorticity lines meet, which by the MRS condition corresponds to the occurrence of the separation singularity. Similarly, the location of the separation singularity is estimated from extrapolated results of the location of the tip of the spike in the numerical solution. The time and location of the separation singularity using this method are estimated to be $t_s = 0.988$ and $\xi_s = 1.133$, which compare well with Lagrangian results[6] of $t_s = 0.989$ and $\xi_s = 1.134$.

Discussion and Summary

The success of the present approach is attributed to the use of the analytical weight function. To resolve large gradients in a flowfield, a weak coupling is important to prevent the grid movement from interfering with the flow solution. An apparent advantage of the present scheme is that a degradation of stability and accuracy are not observed when using standard central difference approximations. Previous investigations[1,6] in both Eulerian and Lagrangian systems are complicated by the use of upwind differencing techniques to prevent a loss of diagonal dominance in the tridiagonal system of linearized difference equations. Finally, it is concluded from Table 3 that the computational cost of managing the grid points is justified. The most significant savings in CPU time and memory are due to the fact that the grid points are only being moved in one dimension, and this fact could surely be exploited in other two- or even three-dimensional problems. Computational efficiency is especially important here since an iterative procedure is required to determine the free parameters of the weight function.

It is concluded that an effective method for resolving singular behavior in an Eulerian coordinate system has been developed. Although the present approach is easy to implement within an Eulerian framework, the adaptive-grid method described here is not designed to identify when a singularity is encountered and therefore, strictly speaking, is not a "numerical proof"[5] of the existence of the singularity. The scheme effectively organizes grid points into the eruptive region of the flow, and the result is that information about the flowfield is resolved (in agreement with Lagrangian and asymptotic results) that is otherwise not obtainable by conventional fixed-grid schemes.

It is important to note that the present method does not require information about the singular time or the position of the singular point in space, although this information may be useful. Indeed, we are now producing solutions for the interacting boundary-layer problem for the impulsively started cylinder for which the singular time is unknown, and the results will be reported in a future paper.

Acknowledgments

This work is supported by the U.S. Army Research Office under Contract DAAL03-92-G-0134; the third author was supported by Contract DAAL03-92-G-0040. The continued support of the contract monitor, T. L. Doligalski, is greatly appreciated. Computations were performed through a grant of computer time from the Ohio Supercomputer Center. Many useful discussions with O. R. Burggraf and Z. Xiao are gratefully acknowledged.

References

[1]Walker, J. D. A., "The Boundary Layer due to a Rectilinear Vortex," *Proceedings of the Royal Society of London, Series A: Mathematical and Physical Sciences*, Vol. 359, 1978, pp. 167–188.

[2]Doligalski, T. L., Smith, C. R., and Walker, J. D. A., "Vortex Interactions with Walls," *Annual Review of Fluid Mechanics*, Vol. 26, 1994, pp. 573–616.

[3]Affes, H., Xiao, Z., and Conlisk, A. T., "The Three-dimensional Boundary Layer Flow due to a Rotor Tip Vortex," AIAA Paper 93-3081, June 1993.

[4]Sears, W. R., and Telionis, D. P., "Unsteady Boundary-Layer Separation," *Recent Research on Unsteady Boundary Layers*, Laval Univ. Press, Quebec, Canada, 1971, pp. 404–447.

[5]Van Dommelen, L. L., and Shen, S. F., "The Spontaneous Generation of the Singularity in a Separating Laminar Boundary Layer," *Journal of Computational Physics*, Vol. 38, 1980, pp. 125–140.

[6]Peridier, V. J., Smith, F. T., and Walker, J. D. A., "Vortex-Induced Boundary-Layer Separation. Part 1. The Unsteady Limit Problem $Re \rightarrow \infty$," *Journal of Fluid Mechanics*, Vol. 232, 1991, pp. 99–131.

[7]Elliott, J. W., Cowley, S. J., and Smith, F. T., "Breakdown of Boundary Layers: (i) On Moving Surfaces; (ii) In Self-Similar Unsteady Flow; (iii) In Fully Unsteady Flow," *Geophysical and Astrophysical Fluid Dynamics*, Vol. 25, 1983, pp. 77–138.

[8]Vickers, I. P., and Smith, F. T., "Theory and Computations for Break-Up of Unsteady Subsonic or Supersonic Separating Flows," *Journal of Fluid Mechanics*, Vol. 268, 1994, pp. 147–173.

[9]Hawken, D. F., Gottlieb, J. J., and Hansen, J. S., "Review of Some Adaptive Node-Movement Techniques in Finite-Element and Finite-Difference Solutions of Partial Differential Equations," *Journal of Computational Physics*, Vol. 95, 1991, pp. 254–302.

[10]Eiseman, P. R., "Adaptive Grid Generation, *Computer Methods in Applied Mechanics and Engineering*, Vol. 64, 1987, pp. 321–376.

[11]Adams, E. C., "Adaptive Grid Methods for Unsteady Problems in Fluid Mechanics," M.S. Thesis, Dept. of Mechanical Engineering, Ohio State Univ., Columbus, OH, 1994.

[12]Harvey, J. K., and Perry, F. J., "Flowfield Produced by Trailing Vortices in the Vicinity of the Ground," *AIAA Journal*, Vol. 9, 1971, pp. 1659–1660.